Quantitative probe of the transition metal redox in battery electrodes through soft x-ray absorption spectroscopy

2016 J. Phys. D: Appl. Phys. 49 413003

(http://iopscience.iop.org/0022-3727/49/41/413003)

IOP Publishing Journal of Physics D: Applied Physics

J. Phys. D: Appl. Phys. **49** (2016) 413003 (14pp) doi:10.1088/0022-3727/49/41/413003

Topical Review

Quantitative probe of the transition metal redox in battery electrodes through soft x-ray absorption spectroscopy

Qinghao Li[1,2], Ruimin Qiao[2], L Andrew Wray[3], Jun Chen[1], Zengqing Zhuo[2,4], Yanxue Chen[1], Shishen Yan[1], Feng Pan[4], Zahid Hussain[2] and Wanli Yang[2]

[1] School of Physics, National Key Laboratory of Crystal Materials, Shandong University, Jinan 250100, People's Republic of China
[2] Advanced Light Source, Lawrence Berkeley National Laboratory, Berkeley, CA 94720, USA
[3] Department of Physics, New York University, New York, NY 10003, USA
[4] School of Advanced Materials, Peking University Shenzhen Graduate School, Shenzhen 518055, People's Republic of China

E-mail: shishenyan@sdu.edu.cn and wlyang@lbl.gov

Received 6 June 2016, revised 26 July 2016
Accepted for publication 1 August 2016
Published 16 September 2016

Abstract

Most battery positive electrodes operate with a 3*d* transition-metal (TM) reaction centre. A direct and quantitative probe of the TM states upon electrochemical cycling is valuable for understanding the detailed cycling mechanism and charge diffusion in the electrodes, which is related with many practical parameters of a battery. This review includes a comprehensive summary of our recent demonstrations of five different types of quantitative analysis of the TM states in battery electrodes based on soft x-ray absorption spectroscopy and multiplet calculations. In $LiFePO_4$, a system of a well-known two-phase transformation type, the TM redox could be strictly determined through a simple linear combination of the two end-members. In Mn-based compounds, the Mn states could also be quantitatively evaluated, but a set of reference spectra with all the three possible Mn valences needs to be deliberately selected and considered in the fitting. Although the fluorescence signals suffer the self-absorption distortion, the multiplet calculations could consider the distortion effect, which allows a quantitative determination of the overall Ni oxidation state in the bulk. With the aid of multiplet calculations, one could also achieve a quasi-quantitative analysis of the Co redox evolution in $LiCoO_2$ based on the energy position of the spectroscopic peak. The benefit of multiplet calculations is more important for studying electrode materials with TMs of mixed spin states, as exemplified by the quantitative analysis of the mixed spin $Na_{2-x}Fe_2(CN)_6$ system. At the end, we showcase that such quantitative analysis could provide valuable information for optimizing the electrochemical performance of $Na_{0.44}MnO_2$ electrodes for Na-ion batteries. The methodology summarized in this review could be extended to other energy application systems with TM redox centre for detailed analysis, for example, fuel cell and catalytic materials.

Keywords: soft x-ray absorption spectroscopy, transition-metal redox, Li-ion batteries, Na-ion batteries

S Online supplementary data available from stacks.iop.org/JPhysD/49/413003/mmedia

(Some figures may appear in colour only in the online journal)

1. Introduction

Developing high-performance energy storage materials and technologies are under pressing demand for today's sustainable energy applications such as electric vehicles (EVs) and electric grid [1–5]. The rechargeable Li-ion battery remains one of the most promising candidates for EVs with high capacity and high power density. The rechargeable Na-ion battery holds the promise of low-cost for grid-scale storage [6, 7]. In the past decades, tremendous research and development efforts have been made to achieve both a systematic understanding and technological optimization of batteries by researchers in the academy, government and industry. Despite all these efforts, technological breakthrough remains formidable to overcome the bottleneck problems related to the battery stability, safety, and cost issues, which are impeding further developments of the battery technology to meet the requirements of large scale EV and grid applications. In the meantime, modern material characterization tools have empowered the researchers in the field with multimodal approaches for both the fundamental understanding and practical optimization of the battery systems. The optimism lies in the hope that systematic and detailed understanding of the evolving material properties and chemistry in batteries could provide the rationality and guideline for technological breakthroughs [2–7].

Among the many technical challenges for realizing a high-performance Li-ion battery, a cathode material that is safe and of high energy density remains elusive. The current cathode component in a commercial battery system is the bottleneck of several practical parameters, especially the storage capacity [8–10]. At this time, most cathode materials are of the so-called intercalation type, which allows the Li-ion (Li^+) insertion and extraction through a more or less open and stable lattice structure. Such widely employed materials are still the most promising cathode technology in the short-/mid-term. Most widely used intercalation type battery materials are 3*d* transition metal (TM) compounds with certain lattice structures as a stable host framework for reversible Li-ion insertion and extraction [8–10]. The electronic state configuration and interplay between TM redox couple and ligand anion 2*p* states fundamentally determine the battery performance related to intrinsic voltage limit and safety, which also gives clues for the intrinsic capacity fading mechanism [3].

In an ideal scenario, TM is the reversible redox centre in a battery cathode. During the electrochemical lithiation and delithiation process, the TMs in cathodes are reduced and oxidized, respectively. While electrochemical and structural characterizations have been extensively employed to study the TM based cathode compounds, the redox reaction is actually an electronic process involving the variation of both the number and reconfiguration of the TM 3*d* electrons. Therefore, a precise analysis of the TM redox at different electrochemical states is indispensable for understanding the material evolution during the battery operation, and more importantly, for revealing the subtle irreversible reactions that impact the battery stability.

Soft x-ray absorption spectroscopy (sXAS) is a direct probe of the excited TM 3*d* states through the dipole allowed 2*p* to 3*d* (L-edge) electron excitations, which fingerprints the formal valence, spin state and chemical bond configuration [11, 12]. There are several unique advantages of TM L-edge for studying battery cathode compounds. First, because the TM L-edge spectral lineshape is defined largely by the atomic multiplet effects, sharp and well-defined features could be observed in sXAS results, which provides the unique opportunity for detailed and quantitative analysis. Second, due to the intrinsically different penetration depth of electrons and photons, the probe depth of sXAS in the electron and photon detection modes ranges from several nanometers to about 150 nm with certain tunability. This enables sXAS as a probe of the contrast between the surface and the bulk in battery materials [13]. Third, sXAS could access the conduction bands of the low *Z* elements such as C, N, and O [14], which are the typical ligand elements in battery materials. This makes it possible to map out both the TM 3*d* and the anion 2*p* states in battery materials, which fundamentally defines the material performance in many aspects [15]. Fourth, with the high brilliance 3rd generation synchrotron facility, it is now possible to utilize sXAS as not only a sensitive and quantitative probe of the TM 3*d* states, but also, sXAS could be performed under *in situ/operando* battery conditions [16–18], and with microscopic capabilities of nanometer scale spatial resolution for imaging battery materials [19].

This review explains the basic principles of different types of quantitative analysis of the TM redox based on sXAS results. We summarize our recent developments on methodologies with demonstrations in battery systems with various 3*d* TM elements, phase transformation, and spin states. Our focus is to demonstrate the power of such quantitative analysis, and how such detailed study of the surface and bulk TM 3*d* states in battery electrodes could lead to deep understanding and sometimes practical optimization of battery operations. Detailed technical discussions on battery materials are not included here in order to limit the scope of this paper, the readers could refer to a number of books and review papers that have been published on x-ray absorption spectroscopy and battery materials [8, 11, 12, 20–23]. In section 2, we will introduce the relevant principles of lithium ion battery operation and sXAS. We explain why the TM L-edge sXAS is principally the tool-of-choice for quantitative studies of TM redox in battery cathode compounds. In section 3, we first showcase the precision of a straightforward quantitative sXAS fittings of the Fe redox in $LiFePO_4$, a material that is known to form a two-phase transformation cathode in electrochemical cycling. We then show that even for a system that is not strictly following two-phase transformation, the same methodology based on a linear combination of more than two involved references could still work for Mn redox analysis in spinel cathode materials. The conventional bulk probe of sXAS through total fluorescence yield suffers the intrinsic lineshape distortion, however, with the aid of multiplet calculations that consider the self-absorption distortion, a quantitative fitting of Ni redox is presented in a $LiNi_{0.5}Mn_{1.5}O_4$ cathode study, where Ni^{3+} is clearly defined for the first time. In contrast, a highly solid-solution type of phase transformation does not allow a simple fitting through linear combination. Instead, we need to utilize

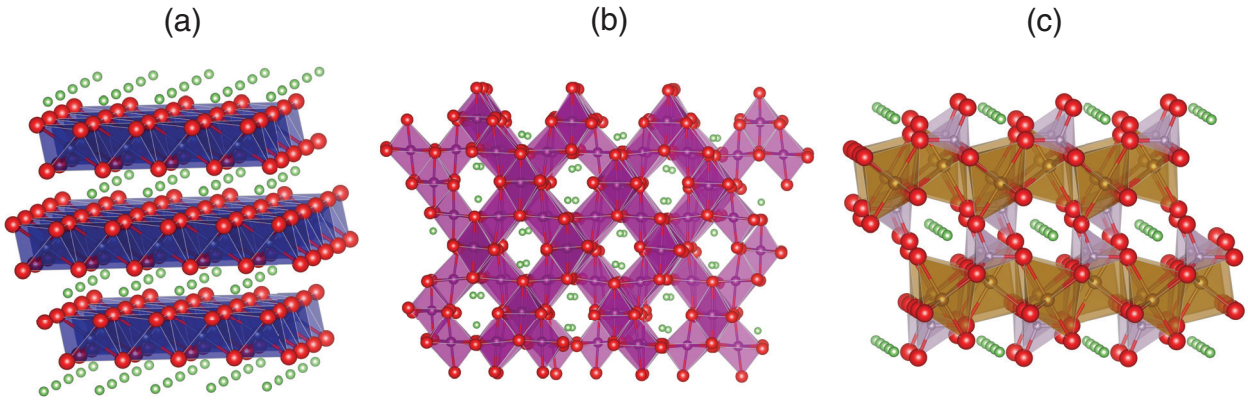

Figure 1. Three typical lattice structure of the intercalation-type cathode materials. (a) layered $LiCoO_2$, (b) spinel $LiMn_2O_4$, (c) olivine $LiFePO_4$, which provides 2D, 3D and 1D lithium diffusion channels, respectively. The host matrix is built up by the corresponding polygons. The green balls represent the Li atoms in the diffusion sites. Reprinted from [21] with permission from Elsevier, copyright 2013.

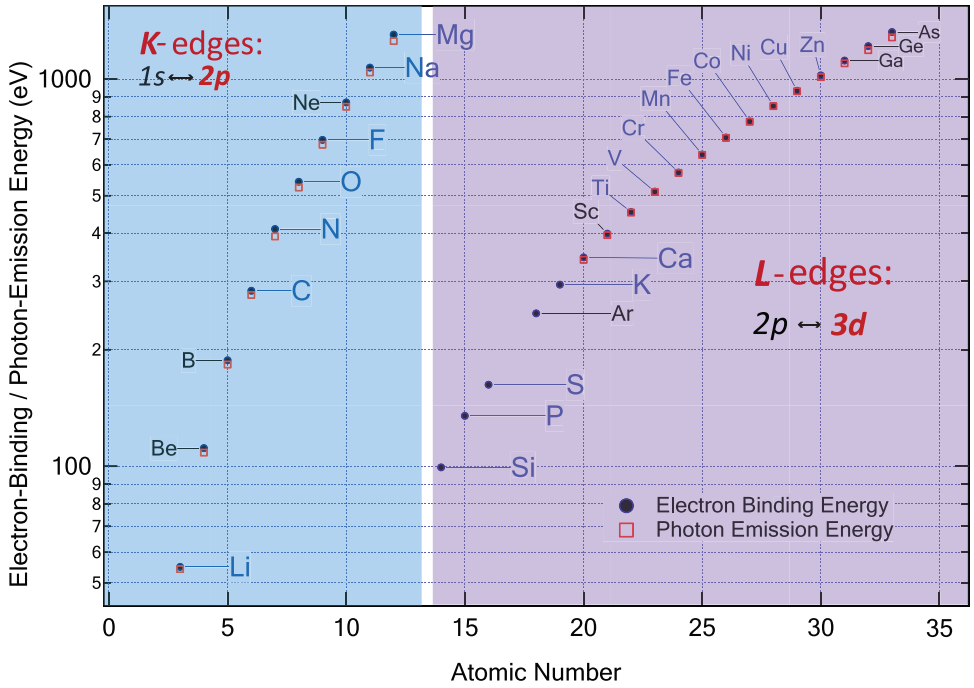

Figure 2. Coverage of elements and corresponding excitations that are accessible by soft x-ray spectroscopy. K- and L-edge spectroscopy detects the 2*p* and 3*d* states of the specific elements, respectively.

the energy values of the sharp feature in sXAS to determine the Co redox in $LiCoO_2$. The aforementioned TM redox analysis is based on single-spin system. In section 4, we present the effect of spin state on battery performance, and show that even with a mixed spin state, the TM redox in batteries could still be distinguished through a combination of sXAS experiments and theoretical simulations. TM atoms coordinated with different ligand elements can be well separated based on different spin state and oxide state. In section 5, we provide an example on the importance of detecting the details of the TM redox. A surface Mn^{2+} formation is revealed on the $Na_{0.44}MnO_2$ material for Na-ion batteries at certain potential range. Avoiding the corresponding electrochemical potential indeed led to the improvement of the cyclability by eliminating the detrimental surface Mn^{2+}. Finally in section 6, conclusive comments are summarized and perspectives of the future applications of sXAS in studying TM based battery materials are discussed.

2. Battery and soft x-ray absorption

The operation of a rechargeable Li-ion battery involves a group of critical components that are constantly under redox reactions: the cathode (positive electrode), the anode (negative electrode) and the electrolyte. The choice of the cathode material directly determines the key parameters of a battery, such as voltage, capacity, and safety. The open circuit voltage of a battery cell is determined by the different lithium chemical potential between the cathode and anode. The capacity depends on the amount of Li diffusion sites, and the accessibility of multiple valence for TM elements in the cathode [3].

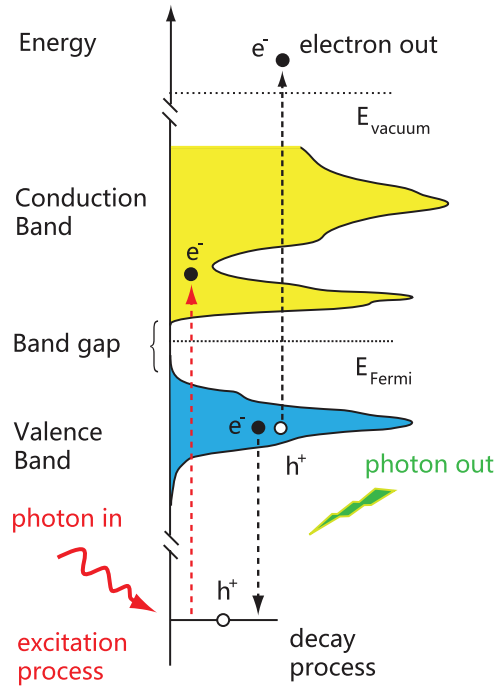

Figure 3. Schematic of the sXAS, which involves excitation of core electron and following decay process. The photon-in–electron-out electron yield is surface sensitive, and photon-in–photon-out fluorescence yield is relatively bulk sensitive, which has formal probe depth of about several nanometers and about 150 nm, respectively. Note that sXAS is a probe of the excited states with a core hole.

The lattice structures of three kinds of typical intercalation-type cathode materials, i.e. the layered structured $LiCoO_2$, spinel $LiMn_2O_4$ and olivine $LiFePO_4$ are shown in figure 1. The layer and spinel structure consists of continuous network of edge-shared TM octahedral arrays as the host matrix, leaving 2D and 3D Li ion diffusion channel respectively. The olivine $LiFePO_4$ features corner-shared TM octahedra that is furthered stabilized by PO_4 tetrahedra, which allows only 1D Li ion diffusion. In intercalation-type batteries, reversible extraction and insertion of Li-ions from/into the cathode host matrix is involved during the electrochemical charge and discharge process, respectively. In order to keep charge neutrality, the Li-ions flow in electrolyte is concerted by electrons shuttling through external circuits. In an ideal case, the cathode is oxidized and holes are introduced to only the TM 3*d* states, increasing the formal valence of TM in the compound during charge process, and vice versa during the discharge.

With TM as the reaction centre, TM 3*d* states are the key evolving electronic states in TM oxides based intercalation type cathode materials. For example, in the case of layered and spinel compounds, the mixed valence TM 3*d* states are critical for improving the electric conductivity, which is an important factor for a cathode material. The battery operation voltage profile can be influenced by the TM redox couple, which is affected by the covalent bonding component and coordination structure (like different polyhedral sites). In order to maximize the cell voltage, higher TM oxidization state within the chemical stability window set by the HOMO (highest occupied molecular orbital) of electrolyte is desirable for cathodes. However, if the energy position of the oxidized TM bands cross the top of the occupied anion 2*p* states, anionic redox will be introduced, which is conventionally considered as detrimental, however, has raised intensive interest recently [24]. Therefore, being able to track the detailed redox evolution of TMs in cathode compounds is of vital importance for understanding and for developments of high-performance battery materials.

Figure 2 shows the electron excitation and photon emission energies that are accessible through soft x-ray absorption and emission process with excitation photon energy of 50 eV to 2 keV. Except for the M- and N-edges of the heavy elements that are not plotted here, sXAS covers the energy range of the 1*s* to 2*p* excitations of the low *Z* elements up to Mg, and as the focus of this review, the 2*p* to 3*d* transitions of the 3*d* TM elements. Therefore, the valence electronic states (2*p* states for low *Z* elements and 3*d* states for 3*d* TMs) can be directly accessed through sXAS via the dipole allowed transitions.

The schematic of sXAS is shown in figure 3, in which a tightly bound core level electron absorbs incident photon energy and gets excited into the empty electronic state above Fermi level. Subsequently, the excited state disposes of the acquired energy by cascade through the fluorescence (photon) or Auger (electron) decay process. Naively, the probability of both decay channels (fluorescence or electron) is proportional to the absorption probability. So the x-ray absorption coefficient can be measured by detecting the total number of either the photon or electron decays. The total electron yield (TEY) is a photon in electron out detection mode (PIEO) with a probe depth of several nanometers due to the shallow escape depth of electrons. Total fluorescence yield (TFY) is a photon in photon out detection mode (PIPO) which is relatively bulk sensitive with probe depth of about 150 nm. While TFY signals suffer the intrinsic saturation effect [25], the contrast between the TEY and TFY signals often provides some qualitative but valuable comparison between the material surface and bulk [26]. In general, even with the about 150 nm probe depth of TFY, sXAS remains a surface sensitive probe compared with the typical thickness of tens of micrometers of a battery electrodes. sXAS could thus enable position dependent studies on different sides of a laminate cathode, which provides information on the lateral gradient distribution of Li-ions in cathode materials [27].

In reality, however, sXAS process involves two important effects. Firstly, sXAS does not measure the unoccupied ground states directly, instead, the transition probability W is governed by the Fermi Golden Rule: $W_{fi} = (2\pi/\hbar)|\langle\Phi_f|T|\Phi_i\rangle|^2\delta(E_f - E_i - \hbar\Omega)$, between the initial state Φ_i and final state Φ_f, with the transition operator T that is regulated by the dipole selection rule. Such a final state effect is critical for the interpretation of the TM L-edge sXAS. The L-edge excitation leads to two partially filled shells, i.e. the $2p^5$ orbital with a core hole and the $3d^{n+1}$ orbital with one extra electron. The overlap between these two states is large, which introduced the strong so-called multiplet features that dominate the TM L-edge sXAS data [11]. Fortunately, the modern sXAS resolution could easily resolve most of the multiplet features in TM L-edge sXAS [11, 12], and even in the anion-TM hybridization states in the fluorine systems [28]. In a typical

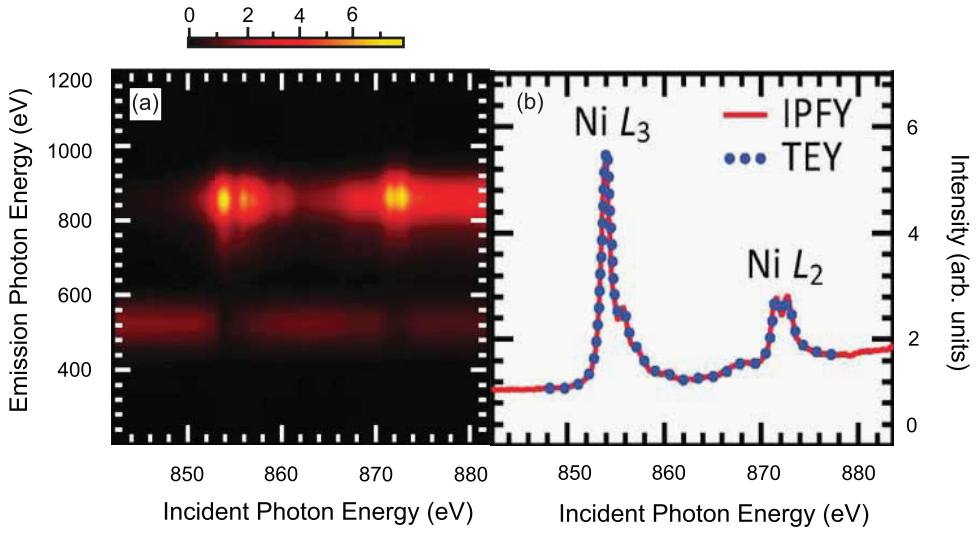

Figure 4. Energy distribution fluorescence yield of NiO. Data were collected with silicon drift detector. (a) Normalized x-ray fluorescence of NiO with the incident photon energy (horizental axis) scan through Ni-L edge and with the emission photon energy (vertical axis) detected by detector. (b) The comparison between the Ni L-edge IPFY (see text) and TEY data of NiO, which is in perfect agreement with each other. Reprinted from [29] with permission from the Nature Publishing Group, copyright 2011.

TM-L edge sXAS, the spectra consists of well separated L_3 and L_2 absorption features in lower and higher absorption photon energy respectively. The splitting of two absorption edges originates from the core-hole spin orbit coupling effect. Owing to the shorter lifetime of the $2p^{1/2}$ core hole, the L_2 edge in higher photon energy generally demonstrates broader features. As a result, the quantitative spectra analysis typically focus on the L_3 edge fine feature. Furthermore, theoretical multiplet calculations of TM L-edge sXAS can often be performed with excellent agreement with experimental data, due to the atomically localized and well defined TM 3*d* states. As shown below, the combination of theoretical calculations and experimental spectra could enable a quantitative analysis of the TM states based on sXAS features in different scenarios even without experimental data from reference samples.

The other technical complication involved in sXAS experiments is the so-called self-absorption effect for data collected in fluorescence mode [25]. Self-absorption effect is due to the abrupt change of the penetration depth of the x-rays when the incident photon energy scans through an absorption edge. Strong peaks are suppressed in the collected spectra and the sXAS lineshape is distorted in the TFY mode with respect to the actual absorption coefficient. In particular, this distortion becomes serious if the edge of interest sits relatively close at a higher energy of another absorption edge. For example, for Mn oxide based materials, because Mn-L (640 eV) sits higher than the O-K (530 eV) in energy, the change of the O-K fluresecence background at the Mn-L absorption energies is strong enough to severely distort the TFY of the Mn L-edge sXAS lineshape. A typical example is shown in [30] on the Mn L-edge of $LiMnO_2$. The spectral distortion in TFY mode seemingly hinders its direct employment in quantitative analysis.

However, there are two ways to compensate the distortion effect in TFY sXAS signals for achieving a quantitative analysis. One is through the theoretical multiplet calculations that consider the self-absorption effect in the TFY mode. As demonstrated later in this review, a reliable calculation could generate the necessary reference spectra with well defined multiplet features for a quantitative fitting of the TFY signal. The other solution is technically based on the recent demonstration of the inverse partial fluorescence yield (IPFY) that is free of self-absorption effects [31]. In contrast to TEY or TFY which is a measure of the number of core-hole excitation through typical absporption edge, IPFY is effectively a measure of the x-ray attenuation length, akin to transmission measurement. Figure 4 demonstrates the extraction of IPFY from a map of energy resolved x-ray emission of NiO with the excitation energy scans through the Ni L-edge through a silicon drift detector by Achkar *et al* [29]. The Ni-L edge x-ray absorption corresponds to Ni 2*p* to 3*d* transition, the incident photon energy is high enough to induce O 1*s* to 2*p* transition. The main features at about 840 eV and 524 eV correspond to the x-ray fluorescence signals of Ni 3*d* to 2*p* transitions and O 2*p* to 1*s* transitions, respectively. It is obvious that the O-K edge emission intensity dips at the energy corresponding to the Ni-L edge absorption. Morever, it is found that the inverse of the O K-edge PFY is linearly proportional to the x-ray absorption coefficient [31]. Figure 4(b) shows that the IPFY spectrum of O-K edge emission agrees precisely with the TEY spectrum. The consistency between TEY and IPFY highlights the ability of bulk sensitive IPFY to measure the absorption coefficient of TM-L edge without self-absorption induced distortion. IPFY could be collected through either silicon drift detector, or high-efficient resonant inelastic x-ray scattering (RIXS) spectrometer that has been realized [32], and it is worthy noting that the same methodology summarized in this review could also be extended to IPFY data for a quantitative analysis of the TM redox in the bulk of electrodes.

3. sXAS of TM 3*d* states in battery cathodes

By virtue of the sensitivity to the TM 3*d* states and the sharp features from multiplet effects, TM L-edge sXAS is arguably

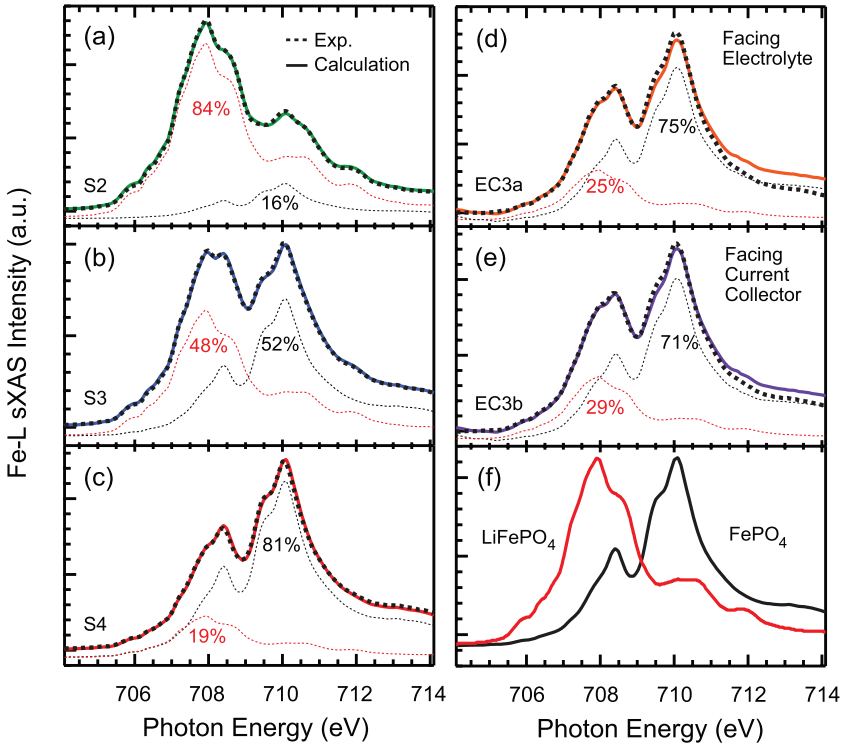

Figure 5. (Left) (a)–(c) Experimental Fe-L edge sXAS (solid line) over-plotted with the simulated spectra (thick dotted black lines) of chemically delithiated Li_xFePO_4, denoted as S2, S3, and S4. The chemical valence states change between Fe^{2+} and Fe^{3+} can be quantitatively obtained with the perfect fitting. (Right) (d) and (e) Experimental and simulated spectra on electrochemical delithiated Li_xFePO_4 cathodes, the spectra are collected on different side of the laminate cathode facing electrolyte separator (d) and facing current collector (e). Compared with the perfect fitting of the data of chemically delithiated S2—4, the fittings of EC3a and EC3b data are less perfect, indicating the subtle deviation from the two-phase transformation in these electrochemically cycled samples. The fitting is through a simple linear combination of the spectra of two end states, i.e. $LiFePO_4$ and $FePO_4$., as shown in (f). Data from [33] with the absolute energy values calibrated.

the most direct probe of the TM redox in battery electrodes. In this session, we will first demonstrate that, in the $LiFePO_4$ electrode system with two-phase transformation, a simple linear combination of the spectra of the two end members, i.e. Li_xFePO_4 ($x = 0$ and 1) could precisely fit the intermediate states for obtaining a quantitative value of the state-of-charge (SOC) the electrodes. This simple analysis could be utilized for *in situ* and microscopic studies. We then show that this simple approach is applicable to Mn-based electrodes that are not strictly under two-phase transformation. While TFY signals cannot be directly used for quantitative analysis as described above, the sXAS feature assignment could easily distinguish the different Ni-redox in battery electrodes. At the end, we show that, with the aid of theoretical multiplet calculation, it is possible to obtain the redox evolution in a highly solid-solution type of cathode system, $LiCoO_2$, by analyzing the energy position of the Co sXAS peaks.

3.1. Fe redox: a precise and quantitative definition in $LiFePO_4$

As one of the safest and environmental benign cathode matreials for EVs, olivine lithium iron phosphate has attracted much research attention. In olivine Li_xFePO_4 cathode, the two phase transformation mechanism during battery operation has been extensively verified through structural probes, which is also indicated by the electrochemical charge/discharge voltage plateau that is independent of x value over a large range of x [34–36]. In the meantime, theoretical and experimental studies suggest that $LiFePO_4$ system may circumambulate the energy barrier for a two-phase process by going through a metastable single phase [37].

The two phase transformation involves compositional change between two end states $LiFePO_4$ and $FePO_4$, which intrinsically allows a linear combination of sXAS spectra of the two end states $LiFePO_4$ and $FePO_4$ for a quantitative spectra simulation. Figure 5 shows the L_3 feature of Fe-L edge sXAS spectra collected in TEY mode (solid line) and corresponding quantitatively fitted spectra (thick dashed line) of partially electrochemically/chemically delithiated $LiFePO_4$. The magnified view of the reference $LiFePO_4$ and $FePO_4$ spectra are attached in supplementary figure S1 (stacks.iop.org/JPhysD/49/413003/mmedia). In the typical Fe-L_3 edge sXAS spectra, the relative change of the two peaks weight (at around 708 eV and 710 eV respectively) indicates the evolution of Fe^{2+} and Fe^{3+} oxide state concentration. A fitting through a simple linear combination of the two end states spectra of $LiFePO_4$ and $FePO_4$ is used to quantify the SOC of the intermediated states. As shown in figures 5(a)–(c), for the chemically delithiated samples, the high resolution and sensitivity of sXAS of Fe L-edge enables a precise reconstruction of all the fine features of experimental spectra, yielding a high-precision definition of the Li content. The fitting

perfectly overlaps with the experimental data even on the fine features, indicating a strict two-phase system for the chemically prepared Li_xFePO_4 [33].

The high-precision quantitative fitting of the multiple chemically prepared samples is in contrast with that of the electrochemically cycled Li_xFePO_4, for which, the fitting is less perfect. The subtle but consistent deviation can be observed on the electrochemical delithiated $LiFePO_4$ between the simulated spectra and experimental data at 709.5 eV in (d) and (e), in contrast to the perfectly fitted spectra on chemically delithiated $LiFePO_4$. Considering the high sensitivity of sXAS to TM 3*d* states and the about 2-folder larger difference than systematic deviation, the weak but consistent deviation provides a spectroscopic indication of the existence of trace amount of intermediate phase or boundary phase in limited region [33]. The contrast between chemically and electrochemically prepared samples implies that the intermediate or boundary phase formation is more favorable in electrochemical process from the non-structural properties point of view, which is consistent with the theoretical speculation that such phase is kinetically driven metastable [37]. Furthermore, the lineshape fitting yields slightly different Li concentration on opposite sides of the cathode. There is more Fe^{2+} component (29%) on the side facing current collector than the side facing electrolyte (25%), which is consistent with the expected lateral distribution gradient of Li in the cathode upon the dynamic electrochemical process. Overall, the quantitative simulation on the sXAS spectra fingerprinted the (de)lithiation process with much detailed information related to Li-ion diffusion gradient, TM valence state and dynamic difference between chemical and electrochemical process.

It is worthy to note that, the high sensitivity and precise definition of the Fe valence state in $LiFePO_4$ through sXAS provides a unique opportunity to detect the SOC distribution, or the Li-ion diffusion dynamics. This has been well utilized in recent *in situ* and microscopic studies of $LiFePO_4$ electrodes [18, 19, 38]. While $LiFePO_4$ has been commercialized at this time, understanding its phase transformation during the electrochemical operation is still an active topic, which triggers new understanding and novel concepts for seeking materials for the next-generation batteries. Quantitative probe of the SOC and Li-ion diffusion through the Fe L-edge sXAS analysis provides valuable information from the spectroscopic point of view [18, 19, 33, 37, 38].

3.2. Mn redox: surface Mn valence contribution on $LiNi_{0.5}Mn_{1.5}O_4$

While the $LiFePO_4$ system is a well-known two-phase transition system in the battery cathode family. Most of battery cathodes operate with more or less a solid solution type during the electrochemical cycling, instead of a two-phase transition. This is favored in batteries because the charge fluctuation in the solid solution type of phase transformation greatly reduces the energy barrier for ion diffusion, and improves the electric conductivity. In many cases, fundamental understanding on detailed mechanism during charge/discharge process is quite opaque or even controversial. A typical example is the Mn

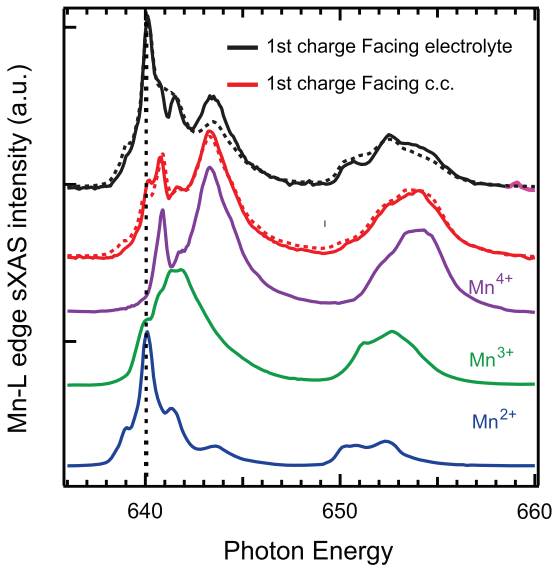

Figure 6. The experimental and fitted Mn L-edge sXAS of a 1st charged $LiNi_{0.5}Mn_{1.5}O_4$ cathode. The 3 spectra on the bottom are selected reference sample spectra of Mn with all the valence states that are involved in the cycling of $LiNi_{0.5}Mn_{1.5}O_4$, Mn^{2+} (MnO), Mn^{3+} (Mn_2O_3) and Mn^{4+} (Li_2MnO_3). The experimental data (solid line) are in good agreement with the simulated spectra (dotted line) which are calculated by a linear combination of all three reference spectra. The contrast between Mn-L edge sXAS collected on the two different sides of the electrode, i.e. the side facing the electrolyte separator or facing the current collector, is obvious, as indicated by the vertical dotted line at 640 eV. Data from [27].

3*d* states which has long been considered critical for understanding capacity fading of spinel electrodes, but the detailed mechanism is still under debate [39]. An important question here is whether the simple linear combination method, which is demonstrated in the two-phase $LiFePO_4$ system, could be extended to the broad range of other cathode compounds that are not strict two-phase systems.

Figure 6 shows the Mn L-edge sXAS spectra of a charged (delithiated) $LiNi_{0.5}Mn_{1.5}O_4$ cathode that shows very poor cyclability during the electrochemical operation [28]. Three reference spectra with different valence states shown as Mn^{2+} (MnO), Mn^{3+} (Mn_2O_3) and Mn^{4+} (Li_2MnO_3) are also plotted [40], with the enlarged view of the Mn-L_3 features shown in supplementary figure S2. Here we focus on the spectral lineshape based on TEY signal, i.e. the surface signal. As shown in figure 6, the spectra of three standard samples with formal valence of Mn^{2+}(MnO), Mn^{3+}(Mn_2O_3) Mn^{4+}(Li_2MnO_3) show dramatically different absorption spectra, again due to the sensitivity of sXAS to the Mn 3*d* states. The linear combination of all the three reference spectra reproduces well the experimental spectra of the cycled $LiNi_{0.5}Mn_{1.5}O_4$, as shown by the dotted lines in figure 6. The overall consistency between the simulated spectra and the experimentally collected sXAS in $LiNi_{0.5}Mn_{1.5}O_4$ cathodes are achieved at different electrochemical states of many electrodes, which validates the reliability of the quantitative analysis of Mn redox based on a linear combination of selected reference spectra. Quantitative spectra simulation based on linear combination of reference spectra empowers researchers to reconstruct the intermediate

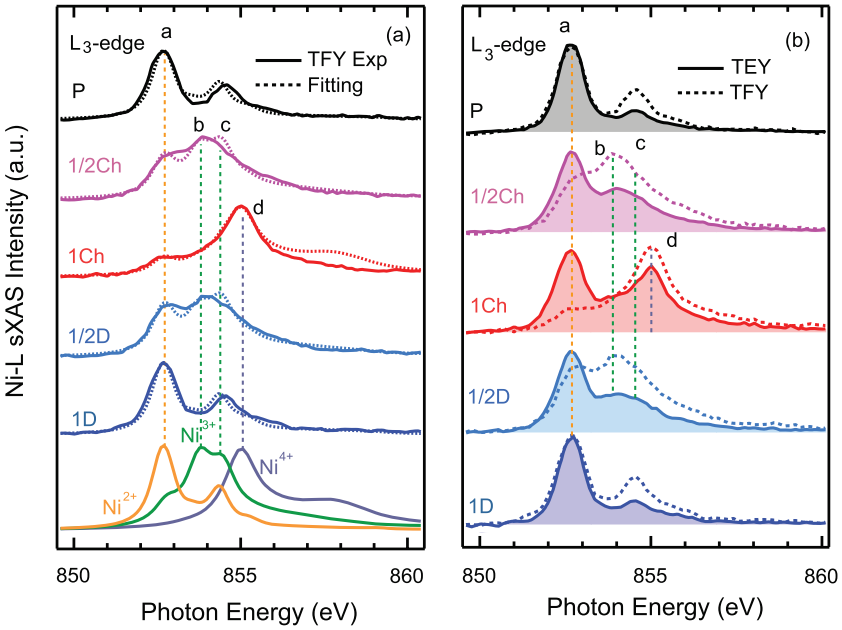

Figure 7. (a) The L_3 features of Ni L-edge sXAS of the $LiNi_{0.5}Mn_{1.5}O_4$ cathodes at different SOC, including pristine (0% SOC), 1/2 charge (50% SOC), 1st charge(100% SOC), 1/2 discharge (50% SOC) and 1st discharge (0% SOC), denoted as P, ½ Ch, 1 Ch, ½ D and 1 D respectively. The experimental sXAS data are shown as the solid line. The fitted spectra are in dotted lines based on a linear combination of the theoretically calculated reference spectra. The theoretical calculation of the Ni spectra with different oxide states, Ni^{2+}, Ni^{3+}, and Ni^{4+}, are displayed at the bottom of panel. The well distinguished features 'b' and 'c' in the 50% SOC samples (1/2 Ch and 1/2 D) are obviously from Ni^{3+}. (b) The comparison between TEY (solid line) and TFY (dotted line) signals of the same batch of samples. All the TEY sXAS spectra show dominant component at low energy around 852.7 eV which originates from Ni^{2+}, in sharp contrast with the TFY spectra. Such contrast between TEY and TFY spectra indicates the existence of electrochemical inactive Ni^{2+} species at the interface. Experimental data are from [41], copyright 2015 American Chemical Society, with the absolute energy values calibrated.

states as well as define and trace TM oxide state with battery evolution.

The analysis shown in figure 6 suggests a counterintuitive and surprising result in two aspects. At the high-voltage charged state, TMs in cathodes should be oxidized to higher oxidation states. While majority of the signal from the side of the electrode attaching to the current collector indeed shows Mn^{4+}, very strong signals of Mn^{2+} can be seen from the side facing the electrolyte separator. Therefore, while the bulk electrode is oxidized at the charged state, as indicated by electrochemical cycling curve, the surface forms low valence Mn^{2+} species on the contrary. The contrast on the surface Mn^{2+} signal of the different side of the electrode indicates the effect of electrolyte. Significant amount of Mn^{2+} is observed on the side facing electrolyte separator. The flourishing of Mn^{2+} in charge (oxidized) state, which can be qualitatively defined by the sharp feature at 640 eV through the spectra fitting (dotted line), demonstrates a strong correlation between the surface TM reduction and the electrolyte degradation at high voltage.

3.3. Ni redox: bulk probe and multiplet calculations

As discussed in section 2, TFY signal of the TM L-edge sXAS of TM oxides provides a bulk probe of the TM redox, however suffers serious self-absorption effect, which distorts the experimental spectra and hinders a straightforward quantitative simulation. However, because the multiplet effect in TM L-edge leads to distinct features in the sXAS spectra, it is possible to achieve a quantitative analysis of the TM redox with the aid of multiplet calculations. Figure 7 shows the comparison of the calculated Ni-L edge spectra with the sXAS data collected in TFY mode as well as the comparison of the sXAS data collected in TEY and TFY mode on $Li_xNi_{0.5}Mn_{1.5}O_4$ cathode material [41]. $LiNi_{0.5}Mn_{1.5}O_4$ is an appealing cathode candidates with high operation voltage of 4.7 V, which is defined by the Ni^{2+}/Ni^{4+} redox couple. However the associated electron transfer process has been elusive on whether it is a single electron or double electron transfer process. With the combination of sXAS and theoretical calculation, the electron transfer process in $Li_xNi_{0.5}Mn_{1.5}O_4$ can be clarified. The figure 7(a) shows the Ni-L edge sXAS collected on a series of $Li_xNi_{0.5}Mn_{1.5}O_4$ electrodes that were electrochemically cycled to different SOC, together with the quantitatively simulated spectra based on theoretically calculated spectra of Ni^{2+}, Ni^{3+} and Ni^{4+} in an octahedral crystal field [41]. The magnified view of the L_3 features of theoretically calculated Ni^{2+}, Ni^{3+} and Ni^{4+} reference spectra are attached in supplementary figure S3. In contrast to the $LiFePO_4$ cathode in which the intermediate states' sXAS TEY spectra can be well reproduced by the linear combination of two end member spectra, the Ni-L edge absorption spectra of $Li_xNi_{0.5}Mn_{1.5}O_4$ electrodes have distinguished features at different photon energy at 50% state of charge from the two end states. As shown in figure 7, the 'b' and 'c' features at half charge or half discharge state shows up at different energy in contrast to the 'a' and 'd' features in pristine or 1st fully charged state. Therefore, the intermediate states of $Li_xNi_{0.5}Mn_{1.5}O_4$ cannot be reproduced by mixing the features of Ni^{2+} and Ni^{4+}, which implies the appearance of a stable intermediate Ni^{3+} valence

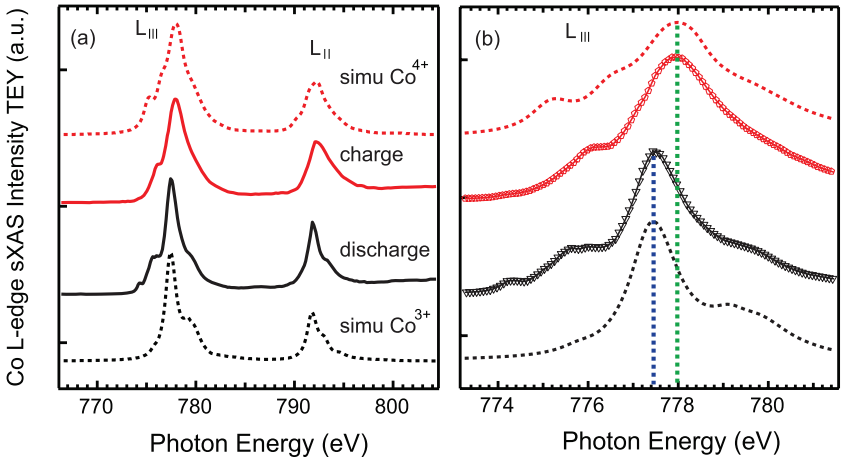

Figure 8. (a) Co L-edge sXAS spectra of $LiCoO_2$ thin films that are electrochemically cycled to the discharge and charge states. Multiplet calculations of the corresponding spectra of $LiCo^{3+}O_2$ and $Co^{4+}O_2$ are displayed in dotted lines. (b) Magnified view of the energy shift of the Co-L_3 peak region, the main peak positions are indicated by the dotted lines.

state at the half charged state. The theoretical calculation based on single impurity Anderson model further proved that the distinguished features denoted as 'b' and 'c' in figure 7(a) come from stable intermediate Ni^{3+} state. Such a quantitative analysis via the combination of experimental sXAS spectra and theoretical calculated spectra provides direct evidence of single electron transfer mechanism and sequence redox reaction of Ni^{2+}/Ni^{3+} and Ni^{3+}/Ni^{4+} can be expected.

On the other hand, the sXAS results collected through the surface sensitive TEY mode show very different spectral lineshape during the charge/discharge process. Figure 7(b) shows the comparison of Ni-L edge sXAS between surface sensitive TEY spectra and bulk sensitive TFY spectra on a series of $Li_xNi_{0.5}Mn_{1.5}O_4$ cathodes, which are electrochemically cycled to different state of charge [41]. With battery operation, the surface layer goes through the same overall electrochemical reaction as that in bulk, i.e. Ni^{2+}/Ni^{3+} to Ni^{3+}/Ni^{4+} redox reaction. However, TEY spectra shows dominating low energy peak denoted as 'a' at all the different SOC, which reveals a significant amount of Ni^{2+} on the cathode surface throughout the battery cycling. The appearance of electrochemical inactive Ni^{2+} state on the electrode surface implies typical interface phenomena like surface rearrangement, electrolyte decomposition and TM dissolution, which is believed to be related to the impedance rise and battery degradation.

With the direct comparison of TEY and TFY signals of sXAS, different TM states between the surface (interface) and the bulk electrode is clearly revealed although TFY signal suffers distortion from self-absorption effect. Additionally, as discussed in section 2, bulk sensitive spectra collected by the IPFY mode through either silicon drift detectors or RIXS spectrometers could serve as a better choice without lineshape distortion for a quantitative analysis of TM redox in the bulk [29, 31].

3.4. Co redox: a solid solution case

Layered $LiCoO_2$ system is the very first Li-ion battery cathode system, however, only about half of the theoretical capacity could be utilized commercially without triggering catastrophic incident. The failure mode of $LiCoO_2$ electrodes at the highly delithiated level is unclear, and general scenario speculates that the Co 3*d* states at a highly delithiated level could drop below that of the O-2*p* states, so the oxygen is destabilized [3]. Therefore, clarifying the Co redox at a full range of electrochemical potential is valuable for understanding the failure mode of this material, and for technological improvements.

The solid solution type of transformation is well established in layered $LiCoO_2$ electrodes. In a solid solution reaction, the incorporation of the Li ion can be thought of as the solution of the guest into the host material, where only one phase is present and continuous change of the main phase occurs with reversible lithiation/delithiation process. The solid solution type transformation is indicated by the electrochemical charge/discharge profile that features slanted and stretch slope, instead of a flat voltage plateau in the two-phase transition. The solid solution type of phase transformation is reinforced by many reports of x-ray diffraction experiments, where the lattice parameters vary continuously with the composition change [42]. Correspondingly, as shown in figure 8, the sXAS spectra on Co-L edge in $LiCoO_2$ cathode displays a continuous shift during the delithiation process, which cannot be simulated through the linear combination method [43]. Figure 8 also shows the theoretically calculated spectra of Co^{3+} and Co^{4+} based on multiplet theory for trigonally distorted CoO_6 octahedron. A magnified view of the L_3 peak shifting is shown in figure 8(b), in which the main peak positions are emphasized by the dotted lines. The enlarged and labeled spectra of L_3 features are further attached in supplementary figure S4. The perfect reconstruction of the overall spectra lineshape and peak position by theoretical calculation validates the Co^{3+} and Co^{4+} states at the discharged and charged electrochemical states, respectively. A quasi-quantitative analysis based on the peak position could also be achieved for the intermediate states.

4. Mixed spin states and electrochemical potentials

In all the TM cathode materials that are discussed above, the TM 3*d* electrons are of single spin state. TMs in cathode

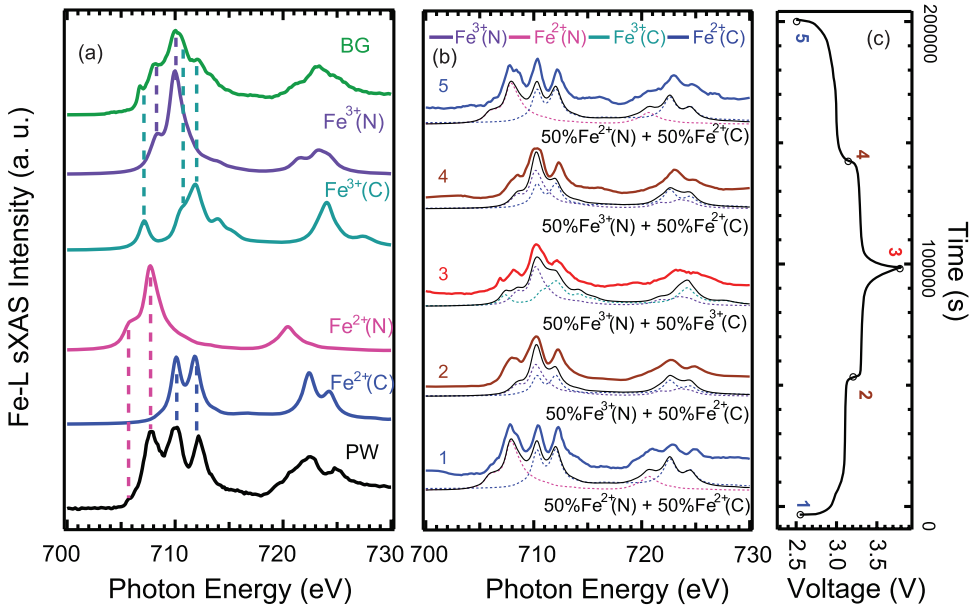

Figure 9. (a) Experimental Fe L-edge sXAS of $Na_{2-x}Fe_2(CN)_6$ Prussian white (PW) and $Fe_2(CN)_6$ Berlin green (BG), compared with the calculated spectra of Fe^{2+} and Fe^{3+} coordinated with C and N sites. The experimental features are well assigned, as indicated by the dashed lines. (b) Fe-L edge sXAS spectra collected on a series of $Na_{2-x}Fe_2(CN)_6$ cathodes that are electrochemically cycled to different SOC, which is indicated by the numbers in (c). The simulated spectra based on the theoretical calculations are shown as the black line in (b). The half charge (2) and half discharge (5) cathodes show no feature at the low energy around 706 eV, indicating thee intermediated states contains only Fe^{3+}(N) and Fe^{2+}(C). Data reprinted with permission from [44], copyright 2015 American Chemical Society, with the absolute energy values calibrated.

compounds could be of mixed spin states, and sometimes even with spin state transition during the electrochemical operations. The different spin state leads to reconfigurations of the TM 3*d* states which fundamentally determines the electrochemical behavior. One important question is whether sXAS could be employed for analyzing the cathode materials with mixed spin states. In principle, because TM L-edge sXAS is a direct probe of the TM 3*d* states, the sXAS spectral lineshape is sensitive to the different spin states. However, experimentally, it is often difficult to obtain a reference sample, i.e. reference spectrum, of a single spin state with a 'correct' chemical phase. Fortunately, the multiplet effect in TM L-edge sXAS results in well-defined features that could be interpreted by multiplet calculation. The assignments of the experimental features to a specific spin state in the battery cathode could clarify the electrochemical cycling mechanism through a combination of sXAS experiments and multiplet theory.

Figure 9 presents an example of mixed spin hexacyanoferrates material developed for Na-ion batteries [44]. The iron atoms in this system are coordinated with the two different C or N sites of the cyano anion groups. The interaction between the Fe atoms and the coordination ligand elements in the polyhedral structure leads to different crystal field strength, which triggers the different spin states of the Fe 3*d* electrons at the two different coordination sites. The electrochemical profile in figure 9(c) clearly shows the two-plateau cycling behavior that corresponds to the two types of iron atoms in different spin states, indicating the spin state of TM could define the electrochemical properties of a cathode material.

Figure 9(a) shows the experimental sXAS spectra on Prussian white $Na_{2-x}Fe_2(CN)_6$ (PW) and Berlin green $Fe_2(CN)_6$ (BG) samples, together with calculated spectra of Fe^{2+} and Fe^{3+} coordinated octahedrally with the C and N sites of the cyano groups. The Fe-L edge sXAS of FeC_6 and FeN_6 octahedra are modeled by multiplet calculations augmented to include both forward and back bonding. For N coordinated Fe sites, the weak ligand field results in simple local physics and sXAS spectra that are characteristic of high spin (HS) state for Fe^{3+}(N) and Fe^{2+}(N), while C coordinated Fe sites display low spin (LS) state of Fe^{3+}(C) and Fe^{2+}(C). As indicated by the dashed vertical lines in figure 9(a), the multiplet calculation successfully assigned all the experimental sXAS features to the different spin states. The magnified view of L_3 feature for corresponding reference spectra are attached in supplementary figure S5. The multiplet calculation shows that the low-energy sXAS feature around 706 eV of the delithiated state is from Fe^{3+}(C). Therefore, the first reduction reaction during an electrochemical lithiation process will be on the Fe atoms at the C sites, which assigns the high-potential cycling plateau to the redox of $Fe^{2+/3+}$(C) [44].

Figure 9(b) shows the Fe-L edge sXAS collected on a series of rhombohedral Prussian white electrodes cycled to different electrochemical states, the corresponding states are marked in the charge-discharge profile in figure 9(c). By the linear combination of the multiplet calculation results, the detailed cycling mechanism on the evolution of Fe states in the charge and discharge process can be clearly explained with the site and spin state sensitivity. As shown in figure 9(b), the calculated spectra (black) agree well with the experimental lineshape. Note that no peak feature can be observed at the low energy around 706 eV in the half charged/discharged states, which indicates the missing components of Fe^{3+}(C) and Fe^{2+}(N). The absence of Fe^{3+}(C) and Fe^{2+}(N) feature provides another direct proof

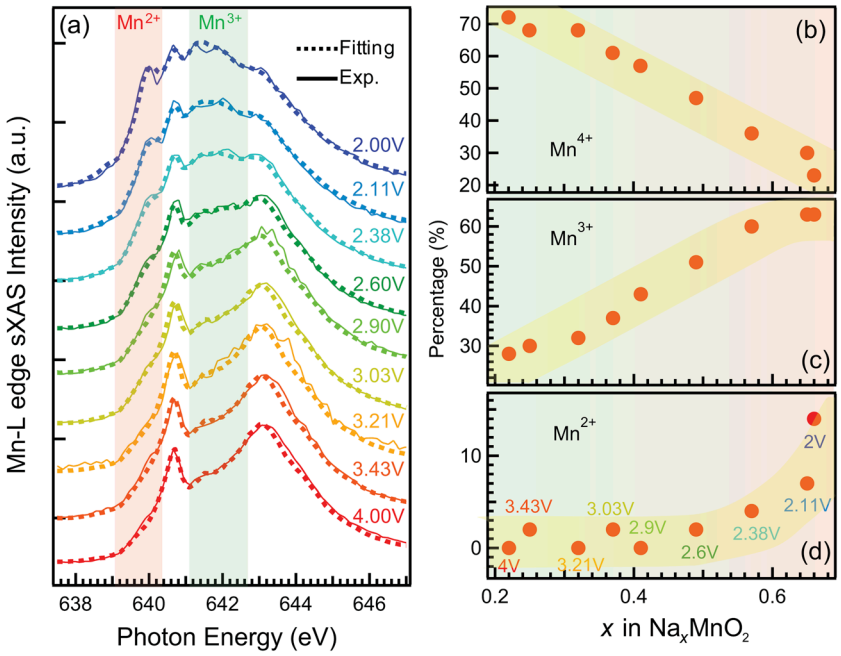

Figure 10. The quantitative analysis of the Mn oxidation state evolution upon the electrochemical potential of the $Na_{0.44}MnO_2$ electrodes in the full cycling potential rang of 2–4V. (a) Comparison between the experimental (solid line) and the simulated (dotted line) sXAS spectra of the $Na_{0.44}MnO_2$ electrodes at the different electrochemical potentials as marked for each spectrum. Data were collected through TEY mode with surface sensitivity. (b)–(d) Quantitative values of the Mn^{4+}, Mn^{3+} and Mn^{2+} concentration from the excellent fittings in (a). The x value of Na_xMnO_2 is calculated based on the cycling capacity. The concentration of the surface Mn^{2+} starts to increase rapidly when the electrochemical potential drops to lower than 2.6V. Reprinted from [46] with permission from the Journal of the American Chemical Society, copyright 2012.

that the low voltage and high voltage plateau in voltage profile corresponds to redox reaction on FeN_6 and FeC_6 octahedral respectively.

The different electrochemical potentials of Fe redox couple in different coordination site can be fundamentally understood from the electron configuration and spin state point of view. High spin Fe^{3+}(N) state shows electronic configuration of t^3e^2, all in majority spin. Adding one more electron with minority spin to such configuration gains no interatomic exchange stabilization while cost higher energy due to electron–electron on-site repulsion effect, which leads to higher unoccupied states in energy scale. However, adding extra electron on LS Fe^{3+}(C) state is favorable in energy due to the one unoccupied state available in LS t^5 configuration. The combination of experimental sXAS spectra and the theoretical calculation validates the correspondence between the different voltage plateau in battery charge/discharge profile and Fe^{2+}/Fe^{3+} redox states with different ligand coordination sites and different spin states.

5. Revealing surface Mn redox for practical improvements

Considering that rechargeable battery operates with evolving electronic states of both cathode and anode, many importance process in electrochemical reaction such as ion desolvation and charge transfer occur at the interface layer. Although thin as several nanometers to tens of nanometers, the interface between electrolyte and electrode material plays an important role in regulating battery performance related to impedance rise, surface corrosion, TM dissolution and battery degradation. For example, the passivating solid-electrolyte interphase (SEI), which provides a battery the necessary kinetic stability outside of the electrochemical window of electrolyte, has been a critical topic in battery research [45]. Understanding the structure and dynamics of the interface layer is of vital importance to both fundamental research and practical application.

As discussed above, the spatial distinction of TM electronic states can be realized by sXAS spectra analysis by either the contrast between TEY and TFY/IPFY signals or the data from different sides of a cathode (facing electrolyte separator or current collector) [27, 41]. Owing to the different penetration depth of electrons and photons, sXAS measured in TEY and TFY mode intrinsically provide information on the surface/interface (probe depth of about 5 nm) and bulk material (probe depth of about 150 nm) respectively. As shown in figure 7 in the case of $LiNi_{0.5}Mn_{1.5}O_4$, although TFY signal is distorted by the self-absorption effect, the contrast between surface and bulk sXAS still manifests strongly, indicating the formation of a significant amount of Ni^{2+} on the surface. The formation of these electrochemical inactive Ni^{2+} and Mn^{2+} gives deep insight into the mechanism related to surface behavior such as TM dissolution, surface passivation layer formation and electrolyte degradation, which are all critical issues in batteries [9, 39, 45]. Additionally, the shallow probe depth of sXAS, compared with the typical thickness of tens of micrometers in a standard laminate cathode, enables the side sensitive measurement of cathode material facing electrolyte or current collector. As shown in figure 6, the side-dependent evolution of the Mn states in $LiNi_{0.5}Mn_{1.5}O_4$ with different SOC can be tracked following the electrochemical cycle profile [28]. The

agreement between Mn-L edge sXAS and simulated spectra based on reference spectra enables quantitative definition of the different Mn states on the side facing electrolyte separator and current collector. The comparative study of sXAS signals on different cathode surface empowers researchers to clarify the charge dynamics during a battery operation, especially through the combined *ex situ* and *in situ*/*operando* studies [18, 38].

The information from a quantitative analysis of the TM states based on sXAS with surface and bulk sensitivity is important for both understanding and optimizing the battery operations. Here we provide an example on how a battery optimization guidelines could be delivered through such detailed analysis.

Figure 10(a) shows a quantitative analysis on Mn L-edge sXAS on a series of $Na_{0.44}MnO_2$ electrode cycled to different electrochemical states [46]. The dotted lines are simulated spectra through the straightforward linear combination of the three reference spectra of Mn^{2+}, Mn^{3+} and Mn^{4+}, as shown in figure 6 [27, 40]. Again, the simulation reproduces all the fine features in the experimental sXAS data, which provides a precise determination of the surface Mn valence distribution at different electrochemical states.

The deduced Mn valence state evolution is plotted in figures 10(b)–(d) upon the electrochemical potential. When the electrode is discharged from 4 V to 2.6 V, the high oxidation Mn^{4+} concentration decreases monotonously, and the Mn^{3+} concentration increases with Na ion insertion, as shown in figure 10(b) and (c). While the $Mn^{3+/4+}$ redox has long been expected for the $Na_{0.44}MnO_2$ based electrodes [47, 48], it is striking to observe a strong surface Mn^{2+} signal through the surface sensitive TEY mode of sXAS. The Mn^{2+} formation can be observed from the low energy pre-edge feature at around 640 eV, which could be seen directly even in the raw data when the cycling potential is low. The comparison between sXAS in TEY mode and hard x-ray Raman scattering spectra further proved that Mn^{2+} formation is only surface behavior [46]. The comparison between the increasing amount of Mn^{2+} concentration and the capacity loss with extended battery cycles demonstrates that the surface Mn^{2+} formation is detrimental and it likely becomes electrochemical inactive after extended cycles, which is responsible for the capacity decay in the $Na_{0.44}MnO_2$ electrodes [46].

A crucial detail on the surface Mn^{2+} formation is revealed through this quantitative analysis: only negligible amount of Mn^{2+} can be detected in the voltage range from 4.0 V to 2.6 V. When the battery is further discharged below 2.6 V, the Mn^{2+} concentration increases rapidly as shown in figure 10(d). Therefore, the formation of the detrimental surface Mn^{2+} could be suppressed by limiting the discharge cut-off voltage higher than 2.6 V, which could hopefully improve the battery capacity retention over extended cycles. Electrochemical cycling tests show a serious capacity decay with the batteries cycled within 4–2 V voltage range with capacity retention of about 88% after 100 cycles. By limiting the discharge cutoff to the pristine voltage of the $Na_{0.44}MnO_2$ material, 3 V, only negligible capacity loss is observed after 100 cycles [46]. Additionally, the Mn L-edge sXAS spectra on the electrodes that are cycled within 4–2 V show a large amount of Mn^{2+} formation on the electrode surface, while the electrodes that are cycled within the designed 4–3 V range show negligible Mn^{2+} feature at about 640 eV, which have also been further quantized by the simple linear combination fittings [46]. The electrochemical detrimental Mn^{2+} state absence at the interface phenomenon is consistent with the enhance capacity retention behavior. Despite other factors that affect the capacity retention for a battery cycling, such as irreversible structural change, suppressing the Mn^{2+} formation on the electrode surface through a rational setup of the electrochemical cycling parameter indeed leads to a dramatic improvement of the battery capacity retention.

This work also suggests that surface modification treatment such as surface coating could be a plausible approach to optimize the electrochemical performance [49, 50], which has not been practiced much on materials for Na-ion batteries. Moreover, it is an interesting contrast that the Mn^{2+} formation takes place at low electrochemical potential on the surface of the $Na_{0.44}MnO_2$ electrode [46], while the surface Mn^{2+} formation on $LiNi_{0.5}Mn_{1.5}O_4$ electrode is enabled by a high electrochemical potential and associated with electrolyte [27]. The different electrochemical states for the surface Mn^{2+} formation implies different mechanism of the Mn^{2+} formation for different battery materials, which remains a critical topic and requires further studies. A quantitative analysis based on Mn L-edge sXAS results, as demonstrated here, could significantly contribute to this important research topic.

6. Summary and perspectives

In this review, we focus on the quantitative analysis of the TM L-edge sXAS of TM oxide based battery cathode materials, which is proved to be a useful tool to understand the fundamental mechanism and guide the technological optimization. In the typical two-phase transformation type $LiFePO_4$, the Fe oxidation state can be precisely calculated and traced during the electrochemical operation through a simple linear combination of the spectra collected from the two end members, $LiFePO_4$ and $FePO_4$. The dominating two-phase transformation principally allows such a straightforward approach and the simulation provides a spectroscopic tool to study the critical Li-ion diffusion mechanism with subtle deviation from the dominating two-phase transformation. The Mn L-edge sXAS of $LiNi_{0.5}Mn_{1.5}O_4$ electrodes at different electrochemical states could be quantitatively analyzed, through a linear combination of three delicately selected references with different Mn formal valences. Although the TFY signal of sXAS is distorted by the self-absorption effect, the distinct sXAS features of Ni L-edge TFY data could be quantitatively analyzed and all features are assigned to different Ni oxidation states with the aid of multiplet calculations. The stable intermediate Ni^{3+} states are clearly resolved, which clarifies the single electron process in $LiNi_{0.5}Mn_{1.5}O_4$ electrode. Additionally, the contrast between the surface and bulk signals indicates the formation of Ni^{2+} on the surface of the electrode that is electrochemically inactive. For the solid solution type transformation in

layered $LiCoO_2$, the Co L-edge sXAS feature shifts with the electrochemical cycling, and can be well defined and reconstructed by theoretical calculations. Furthermore, such quantitative analysis of sXAS could be extended to electrode systems with mixed spin states, which is exemplified by the site and spin-state sensitive results of Fe 3*d* state in a Na-ion battery material, $Na_{2-x}Fe_2(CN)_6$. The two-plateau electrochemical behavior could be well understood through the detailed sXAS analysis. The quantitative analysis of sXAS with surface and bulk signal contrast contributes to the understanding of the critical interface behaviors in batteries. A comprehensive and quantitative sXAS analysis of the surface Mn evolution on $Na_{0.44}MnO_2$ based electrodes reveals the detrimental surface Mn^{2+} formation at a specific electrochemical potential range. This finding leads to a rational guideline to limit the electrochemical potential lower cutoff voltage, which is demonstrated to be an efficient way for suppressing the surface Mn^{2+} formation and for improving the capacity retention after extended cycles of the battery.

We note that this review is just a tip of the iceberg on the power of quantitative analysis of the TM redox through sXAS. Such a simple analysis could empower researchers to gain detailed and new insights into the battery operation mechanism with valence, spin state, ligand coordination and interface/bulk sensitivity. With the rapid development of synchrotron-based soft x-ray spectroscopy, such as the IPFY [29, 31], high-efficiency RIXS [32], the *in situ*/*operando* soft x-ray instrumentation [51–54], together with the optimization of theoretical calculations, this methodology will continue to be optimized, will play an important role in advancing the battery technology, and will become more and more valuable for studying materials for other energy applications with a TM reaction center.

Acknowledgments

This work is supported by the key program of NSFC No. 11434006, and the 111 project No. B13029. sXAS data were collected at beamline 8.0.1 of the Advanced Light Source, which is supported by the Director, Office of Science, Office of Basic Energy Sciences, of the U.S. Department of Energy under Contract No. DE-AC02-05CH11231. The calculation works are supported by the MRSEC Program of the National Science Foundation under Award Number DMR-1420073. QL thanks the financial support from the China Scholarship Council (CSC).

References

[1] Nykvist B and Nilsson M 2015 Rapidly falling costs of battery packs for electric vehicles *Nat. Clim. Change* **5** 329–32
[2] Armand M and Tarascon J M 2008 Building better batteries *Nature* **451** 652–7
[3] Goodenough J B and Kim Y 2010 Challenges for rechargeable Li batteries *Chem. Mater.* **22** 587–603
[4] Goodenough J B and Park K S 2013 The Li-ion rechargeable battery: a perspective *J. Am. Chem. Soc.* **135** 1167–76
[5] Winter M and Brodd R J 2004 What are batteries, fuel cells, and supercapacitors? *Chem. Rev.* **104** 4245–70
[6] Dunn B, Kamath H and Tarascon J-M 2011 Electrical energy storage for the grid: a battery of choices *Science* **334** 928–35
[7] Yang Z, Zhang J, Kintner-Meyer M C, Lu X, Choi D, Lemmon J P and Liu J 2011 Electrochemical energy storage for green grid *Chem. Rev.* **111** 3577–613
[8] Ellis B L, Lee K T and Nazar L F 2010 Positive electrode materials for Li-ion and Li-batteries *Chem. Mater.* **22** 691–714
[9] Whittingham M S 2004 Lithium batteries and cathode materials *Chem. Rev.* **104** 4271–302
[10] Fergus J W 2010 Recent developments in cathode materials for lithium ion batteries *J. Power Sources* **195** 939–54
[11] de Frank G 2005 Multiplet effects in x-ray spectroscopy *Coord. Chem. Rev.* **249** 31–63
[12] de Groot F and Kotani A 2008 *Core Level Spectroscopy of Solids* (Boca Raton, FL: CRC Press)
[13] Qiao R, Lucas I T, Karim A, Syzdek J, Liu X, Chen W, Persson K, Kostecki R and Yang W 2014 Distinct solid-electrolyte-interphases on Sn (1 0 0) and (0 0 1) electrodes studied by soft x-ray spectroscopy *Adv. Mater. Interface* **1** 1300115
[14] Qiao R, Chuang Y D, Yan S and Yang W 2012 Soft x-ray irradiation effects of Li_2O_2, Li_2CO_3 and Li_2O revealed by absorption spectroscopy *PLoS One* **7** e49182
[15] Liu X *et al* 2015 Why $LiFePO_4$ is a safe battery electrode: Coulomb repulsion induced electron-state reshuffling upon lithiation *Phys. Chem. Chem. Phys.* **17** 26369–77
[16] Arthur T S, Glans P-A, Matsui M, Zhang R, Ma B and Guo J 2012 Mg deposition observed by *in situ* electrochemical Mg K-edge x-ray absorption spectroscopy *Electrochem. Commun.* **24** 43–6
[17] Liu X, Yang W and Liu Z 2014 Recent progress on synchrotron-based *in situ* soft x-ray spectroscopy for energy materials *Adv. Mater.* **26** 7710–29
[18] Li Y, Weker J N, Gent W E, Mueller D N, Lim J, Cogswell D A, Tyliszczak T and Chueh W C 2015 Dichotomy in the lithiation pathway of ellipsoidal and platelet $LiFePO_4$ particles revealed through nanoscale operando state-of-charge imaging *Adv. Funct. Mater.* **25** 3677–87
[19] Li Y *et al* 2014 Current-induced transition from particle-by-particle to concurrent intercalation in phase-separating battery electrodes *Nat. Mater.* **13** 1149–56
[20] Wanli Yang R Q 2016 Soft x-ray spectroscopy for probing electronic and chemical states of battery materials *Chin. Phys.* B **25** 17104
[21] Yang W, Liu X, Qiao R, Olalde-Velasco P, Spear J D, Roseguo L, Pepper J X, Chuang Y-d, Denlinger J D and Hussain Z 2013 Key electronic states in lithium battery materials probed by soft x-ray spectroscopy *J. Electron. Spectrosc. Relat. Phenom.* **190** 64–74
[22] Kim T-H, Park J-S, Chang S K, Choi S, Ryu J H and Song H-K 2012 The current move of lithium ion batteries towards the next phase *Adv. Energy Mater.* **2** 860–72
[23] Scrosati B and Garche J 2010 Lithium batteries: Status, prospects and future *J. Power Sources* **195** 2419–30
[24] Grimaud A, Hong W T, Shao-Horn Y and Tarascon J M 2016 Anionic redox processes for electrochemical devices *Nat. Mater.* **15** 121–6
[25] Eisebitt S, Boske T, Rubensson J and Eberhardt W 1993 Determination of absorption coefficients for concentrated samples by fluorescence detection *Phys. Rev.* B **47** 14103–9
[26] Lin F, Markus I M, Nordlund D, Weng T C, Asta M D, Xin H L and Doeff M M 2014 Surface reconstruction and chemical evolution of stoichiometric layered cathode materials for lithium-ion batteries *Nat. Commun.* **5** 3529

[27] Qiao R, Wang Y, Olalde-Velasco P, Li H, Hu Y-S and Yang W 2015 Direct evidence of gradient Mn(II) evolution at charged states in $LiNi_{0.5}Mn_{1.5}O_4$ electrodes with capacity fading *J. Power Sources* **273** 1120–6
[28] Olalde-Velasco P, Jimeacutenez-Mier J, Denlinger J and Yang W-L 2013 Atomic multiplets at the $L_{2,3}$ edge of 3*d* transition metals and the ligand K edge in x-ray absorption spectroscopy of ionic systems *Phys. Rev.* B **87** 245136
[29] Achkar A J, Regier T Z, Monkman E J, Shen K M and Hawthorn D G 2011 Determination of total x-ray absorption coefficient using non-resonant x-ray emission *Sci. Rep.* **1** 182
[30] Wadati H, Achkar A J, Hawthorn D G, Regier T Z, Singh M P, Truong K D, Fournier P, Chen G, Mizokawa T and Sawatzky G A 2012 Utility of the inverse partial fluorescence for electronic structure studies of battery materials *Appl. Phys. Lett.* **100** 193906
[31] Achkar A J, Regier T Z, Wadati H, Kim Y J, Zhang H and Hawthorn D G 2011 Bulk sensitive x-ray absorption spectroscopy free of self-absorption effects *Phys. Rev.* B **83** 081106
[32] Fuchs O *et al* 2009 High-resolution, high-transmission soft x-ray spectrometer for the study of biological samples *Rev. Sci. Instrum.* **80** 063103
[33] Liu X *et al* 2012 Phase transformation and lithiation effect on electronic structure of Li_xFePO_4: an in-depth study by soft x-ray and simulations *J. Am. Chem. Soc.* **134** 13708–15
[34] Andersson A S, Kalska B, Haggstrom L and Thomas J O 2000 Lithium extraction/insertion in $LiFePO_4$: an x-ray diffraction and Mossbauer spectroscopy study *Solid State Ion.* **130** 41–52
[35] Laffont L, Delacourt C, Gibot P, Wu M Y, Kooyman P, Masquelier C and Tarascon J M 2006 Study of the $LiFePO_4$/$FePO_4$ two-phase system by high-resolution electron energy loss spectroscopy *Chem. Mater.* **18** 5520–9
[36] Yamada A, Koizumi H, Nishimura S I, Sonoyama N, Kanno R, Yonemura M, Nakamura T and Kobayashi Y 2006 Room-temperature miscibility gap in Li_xFePO_4 *Nat. Mater.* **5** 357–60
[37] Malik R, Zhou F and Ceder G 2011 Kinetics of non-equilibrium lithium incorporation in $LiFePO_4$ *Nat. Mater.* **10** 587–90
[38] Liu X, Wang D, Liu G, Srinivasan V, Liu Z, Hussain Z and Yang W 2013 Distinct charge dynamics in battery electrodes revealed by *in situ* and operando soft x-ray spectroscopy *Nat. Commun.* **4** 2568
[39] Gummow R J, de Kock A and Thackeray M M 1994 Improved capacity retention in rechargeable 4 V lithium/lithium-manganese oxide (spinel) cells *Solid State Ion.* **69** 59–67
[40] Qiao R, Chin T, Harris S J, Yan S and Yang W 2013 Spectroscopic fingerprints of valence and spin states in manganese oxides and fluorides *Curr. Appl. Phys.* **13** 544–8
[41] Qiao R, Wray L A, Kim J-H, Pieczonka N P W, Harris S J and Yang W 2015 Direct experimental probe of the Ni(II)/Ni(III)/Ni(IV) redox evolution in $LiNi_{0.5}Mn_{1.5}O_4$ electrodes *J. Phys. Chem.* C **119** 27228–33
[42] Amatucci G G, Tarascon J M and Klein L C 1996 CoO_2, The end member of the Li_xCoO_2 solid solution *J. Electrochem. Soc.* **143** 1114–23
[43] Li Q, Wray L A, Yan S and Yang W 2016 Delithiation effect on the electron states of $LiCoO_2$ electrodes: a study by soft x-ray absorption and emission spectroscopy with theoretical calculations to be submitted
[44] Wang L *et al* 2015 Rhombohedral prussian white as cathode for rechargeable sodium-ion batteries *J. Am. Chem. Soc.* **137** 2548–54
[45] Xu K 2004 Nonaqueous liquid electrolytes for lithium-based rechargeable batteries *Chem. Rev.* **104** 4303–418
[46] Qiao R *et al* 2015 Revealing and suppressing surface Mn(II) formation of $Na_{0.44}MnO_2$ electrodes for Na-ion batteries *Nano Energy* **16** 186–95
[47] Kim H, Kim D J, Seo D-H, Yeom M S, Kang K, Kim D K and Jung Y 2012 *Ab initio* study of the sodium intercalation and intermediate phases in $Na_{0.44}MnO_2$ for sodium-ion battery *Chem. Mater.* **24** 1205–11
[48] Kruk I, Zajdel P, van Beek W, Bakaimi I, Lappas A, Stock C and Green M A 2011 Coupled commensurate cation and charge modulation in the tunneled structure, $Na_{0.40(2)}MnO_2$ *J. Am. Chem. Soc.* **133** 13950–6
[49] Jung Y S, Cavanagh A S, Gedvilas L, Widjonarko N E, Scott I D, Lee S-H, Kim G-H, George S M and Dillon A C 2012 Improved functionality of lithium-ion batteries enabled by atomic layer deposition on the porous microstructure of polymer separators and coating electrodes *Adv. Energy Mater.* **2** 1022–7
[50] Liu J and Manthiram A 2009 Understanding the improvement in the electrochemical properties of surface modified 5 V $LiMn_{1.42}Ni_{0.42}Co_{0.16}O_4$ spinel cathodes in lithium-ion cells *Chem. Mater.* **21** 1695–707
[51] Jeyachandran Y L *et al* 2014 Ion-solvation-induced molecular reorganization in liquid water probed by resonant inelastic soft x-ray scattering *J. Phys. Chem. Lett.* **5** 4143–8
[52] Blum M *et al* 2009 Solid and liquid spectroscopic analysis (SALSA)—a soft x-ray spectroscopy endstation with a novel flow-through liquid cell *Rev. Sci. Instrum.* **80** 123102–6
[53] Weinhardt L, Blum M, Fuchs O, Benkert A, Meyer F, Bär M, Denlinger J D, Yang W, Reinert F and Heske C 2013 RIXS investigations of liquids, solutions, and liquid/solid interfaces *J. Electron. Spectrosc. Relat. Phenom.* **188** 111–20
[54] Guo J 2013 The development of *in situ* photon-in/photon-out soft x-ray spectroscopy on beamline 7.0.1 at the ALS *J. Electron. Spectrosc. Relat. Phenom.* **188** 71–8